⁶Mixing in a Salinity Variance Budget of the Salish Sea is Controlled by River Flow

ERIN M. BROATCH^a AND PARKER MACCREADY^a

^a University of Washington, Seattle, Washington

(Manuscript received 16 October 2021, in final form 20 May 2022)

ABSTRACT: A salinity variance framework is used to study mixing in the Salish Sea, a large fjordal estuary. Output from a realistic numerical model is used to create salinity variance budgets for individual basins within the Salish Sea for 2017–19. The salinity variance budgets are used to quantify the mixing in each basin and estimate the numerical mixing, which is found to contribute about one-third of the total mixing in the model. Whidbey Basin has the most intense mixing, due to its shallow depth and large river flow. Unlike in most other estuarine systems previously studied using the salinity variance method, mixing in the Salish Sea is controlled by the river flow and does not exhibit a pronounced spring–neap cycle. A "mixedness" analysis is used to determine when mixed water is expelled from the estuary. The river flow is correlated with mixed water removal, but the coupling is not as tight as with the mixing. Because the mixing is so highly correlated with the river flow, the long-term average approximation $M = Q_r s_{out} s_{in}$ can be used to predict the mixing in the Salish Sea and Puget Sound with good accuracy, even without any temporal averaging. Over a 3-yr average, the mixing in Puget Sound is directly related to the exchange flow salt transport.

KEYWORDS: Ocean; Estuaries; Buoyancy; Mixing: Budgets; Time series; Numerical analysis/modeling; Regional models

1. Introduction

A defining feature of estuaries is the exchange flow, which draws ocean water into the estuary at depth and expels brackish water near the surface. Two factors are required for the development of an exchange flow: a source of buoyancy and mixing (MacCready et al. 2018). Typically the buoyancy is supplied by rivers, although other sources such as strong precipitation are also possible, and mixing is provided primarily by tides.

Historically, mixing in estuaries has been quantified using buoyancy flux (e.g., Peters and Bokhorst 2001; Simpson et al. 1990), which is a measure of potential energy creation through the destruction of vertical stratification. However, buoyancy flux does not incorporate the effects of horizontal mixing. Moreover, the buoyancy flux for convective mixing and shear-driven mixing will have opposite signs, such that these two mixing modes may cancel each other's contribution to the overall buoyancy flux (Burchard et al. 2009; MacCready et al. 2018; Burchard et al. 2019). Other measures of mixing used in the open ocean such as the turbulent dissipation are important, but not directly useful, in estuarine and coastal environments. Dissipation destroys kinetic energy through turbulence, but may not produce mixing if the water is already well mixed. Similarly, the eddy diffusivity alone is not a suitable measure of mixing, since the mixing also depends on the strength of salinity gradients in the estuary.

More recently, destruction of salinity variance has been used to quantify mixing in estuaries, although loss of tracer

Openotes content that is immediately available upon publication as open access.

Corresponding author: Erin M. Broatch, ebroatch@uw.edu

variance has been used to define mixing in the ocean turbulence field for many decades (Wang and Geyer 2018). Burchard and Rennau (2008) showed that tracer variance decay is a physically sound measure of mixing equivalent to the dissipation of microstructure variance. Salt is an appropriate tracer to choose since it is a conservative tracer and the main driver of density differences in estuarine environments. Therefore, loss of salinity variance is an unambiguous measure that represents irreversible mixing (MacCready et al. 2018; Warner et al. 2020).

Burchard et al. (2009) used both the vertically integrated decay of salinity variance and the vertically integrated turbulent salt flux to quantify mixing associated with dense bottom currents in the western Baltic Sea. They found good qualitative agreement between the two methods for identifying mixing hotspots from model results, because convective mixing is relatively unimportant in the study region. An early study to use the dissipation of salinity variance to quantify mixing in an estuarine context was Wang et al. (2017). Using a numerical model of the Hudson estuary, they found that the mixing is lowest at spring tide, and greatest in the neap-to-spring transition, even though the most energetic turbulence occurs during spring tides. This is because the estuary is restratified around neap tide, so the neap-to-spring transition period has intensified turbulence and strong salinity gradients, which are both required for mixing. Li et al. (2018) decomposed the salinity variance into horizontal and vertical components, which can be used to link four defining estuarine features. 1) The horizontal variance represents horizontal density gradients, which provide a baroclinic pressure gradient that drives the exchange flow. 2) The vertical variance represents stratification. 3) The conversion from horizontal to vertical variance represents straining, and 4) as we have seen previously, the destruction of variance represents mixing. They used this

DOI: 10.1175/JPO-D-21-0227.1

^{© 2022} American Meteorological Society. For information regarding reuse of this content and general copyright information, consult the AMS Copyright Policy (www.ametsoc.org/PUBSReuseLicenses).

framework to evaluate straining and dissipation in the Changjiang estuary.

MacCready et al. (2018) used salinity variance to connect mixing to the magnitude of the estuarine exchange flow. The Knudsen relations (Knudsen 1900; Burchard et al. 2018) relate the magnitude of a time-averaged, two-layer exchange flow to the river flow through the salinities of the inflowing and outflowing layer. By combining the salinity variance budget with a time-dependent version of the Knudsen relations, MacCready et al. (2018) established an approximation for the total mixing using the total exchange flow (TEF) variables. Over a long-term average, such that the storage term in the salinity variance budget becomes small relative to the advection and mixing terms, this approximation can be reduced to a simple relationship $M = Q_r s_{out} s_{in}$, where M is the volumeintegrated rate of salinity variance destruction (mixing), Q_r is the river flow and s_{in} and s_{out} are the inflowing and outflowing salinities, respectively, for an equivalent two-layer exchange flow. Alternatively, this can be expressed as $M = Q_{in}\Delta s s_{in}$, where $Q_{\rm in}$ is the magnitude of the inflowing branch of the exchange flow and $\Delta s = s_{in} - s_{out}$. This formulation links the mixing in an estuary to the strength of its exchange flow, represented by $Q_{\rm in}$, albeit with some ambiguity, since the mixing also affects Δs . MacCready et al. (2018) used an idealized model which, similarly to Wang et al. (2017), shows that mixing peaks just after neap tide. Wang and Geyer (2018) used the salinity variance method to study the effects of varying river flow and the spring-neap cycle on mixing and the exchange flow in the Hudson estuary. By running their numerical model with different levels of constant river discharge, they found that increased river flow leads to increased mixing in the estuary.

Another useful application of salinity variance is that it can be used to diagnose the numerical mixing in a model. Numerical mixing is often overlooked in ocean models, but can significantly impact model results (Ralston et al. 2017). Coarse model grid sizes, sharp gradients, high fluid velocities, and steep bathymetry are factors that may lead to intensified numerical mixing (Ralston et al. 2017), in addition to the choice of advection scheme. As described in Burchard and Rennau (2008), the numerical mixing, defined as the loss of tracer variance due to discretization errors, is equal to the decay rate between the advected square of the tracer and the square of the advected tracer. This method can be used to calculate the numerical mixing in a model on a cell-by-cell basis. Alternatively, the volume-integrated numerical mixing can be estimated as the residual of a salinity variance budget (MacCready et al. 2018), which is appropriate when the model output data capture typical flow time scales (Wang et al. 2021). The volumeintegrated numerical mixing can also be calculated from the diahaline diffusive salt flux and volume-integrated salinity variance dissipation, as described in Wang et al. (2017).

Most of the studies described above used idealized models or models of shallow coastal plain estuaries. We will use the salinity variance framework to study mixing in the Salish Sea, a complex fjordal estuary. The Salish Sea is an inland sea in British Columbia and Washington, which comprises the Strait of Juan de Fuca, Strait of Georgia, and Puget Sound.

The Salish Sea is substantially different from other estuaries previously studied using salinity variance. It is a large, deep fjordal estuary carved by glaciers, with a surface area of approximately 17 000 km² and depths exceeding 400 m in the Strait of Georgia (SeaDoc Society 2021). The Salish Sea is a complex network of interconnected basins, with over 400 islands. Unlike most estuaries, many rivers of varying sizes feed the Salish Sea, and are distributed along its coastline. It is filled with mostly ocean water and therefore very salty, with a mean salinity over 30 g kg⁻¹ in 2017–19. In many regards, the Salish Sea lacks resemblance to simpler estuaries such as the Hudson River. Despite these differences, it still develops one of the largest estuarine exchange flows on the planet (MacCready et al. 2021) and has many qualities characteristic of estuarine systems.

In section 2, we will outline the theory behind the salinity variance framework, as well as the related concept of mixedness. In section 3, we will describe the model and methods used to construct the salinity variance budget, as well as the calculation of mixedness and time series of external forcing factors. Our main goals are to use salinity variance to answer the questions:

- Where and when is mixed water created in the Salish Sea?
- When is mixed water removed from the estuary?
- How well does the long-term average mixing approximation perform in the Salish Sea and Puget Sound?
- How important is numerical mixing in the model?

In section 4 we will discuss the results pertaining to these questions. In section 5 we will summarize conclusions.

2. Theory

a. Salinity variance

The salinity variance in a given volume V is defined as

$$var(s) = \int_{V} s^{r^2} dV, \tag{1}$$

where $s' = s - \bar{s}$, with s being the local salinity and \bar{s} being the mean salinity in the volume. We will call s'^2 the "local salinity variance," acknowledging that while the variance is only defined as a single statistic for the entire volume, s'^2 determines the local contribution to the overall variance when volume integrated. Following MacCready et al. (2018) we start with a salt budget:

$$\frac{\partial s}{\partial t} + \mathbf{u} \cdot \nabla s = \nabla \cdot (\mathbf{K} \cdot \nabla s), \tag{2}$$

where $\mathbf{u} = (u, v, w)$ is the velocity, and $\mathbf{K} = (K_H, K_H, K_V)$ is the eddy diffusivity, with horizontal eddy diffusivity K_H and the vertical eddy diffusivity K_V . Expanding $s = \overline{s} + s'$ and multiplying both sides by 2s', we obtain an equation for the evolution of local salinity variance:

$$\frac{\partial}{\partial t}(s'^2) + \mathbf{u} \cdot \nabla(s'^2) = \nabla \cdot [\mathbf{K} \cdot \nabla(s'^2)] - 2\mathbf{K} \cdot (\nabla s')^2 - 2s' \frac{\partial \overline{s}}{\partial t},$$
(3)

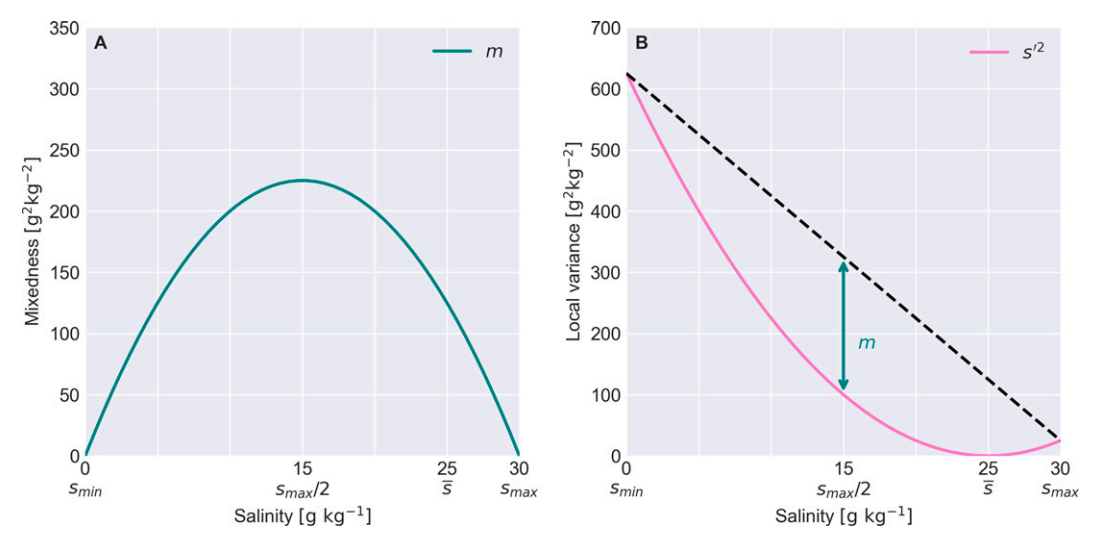


FIG. 1. Example graph explaining (a) mixedness concept and (b) its relationship to salinity variance for a scenario with $s_{\text{max}} = 30$, $s_{\text{min}} = 0$, and $\bar{s} = 25$. Note that $\bar{s} \neq s_{\text{max}}/2$. Since \bar{s} is close to s_{max} , the local variance in this scenario is greatest for the freshwater rivers. This is similar to the situation in the Salish Sea.

where here we use $(\nabla s')^2$ to denote the vector $[(ds'/dx)^2, (ds'/dy)^2, (ds'/dz)^2]$. Now we take the volume integral over the entire estuarine volume V and apply the Reynolds transport theorem. Assuming incompressible flow and that the diffusive transport of salinity variance across the open boundaries is negligible compared to the advective transport, we arrive at the equation for the salinity variance budget:

$$\frac{d}{dt} \int_{V} s'^{2} dV = - \int_{A} s'^{2} \mathbf{u} \cdot \hat{\mathbf{n}} dA - 2 \int_{V} \mathbf{K} \cdot (\nabla s')^{2} dV. \tag{4}$$

The term on the left-hand side represents the time evolution of the variance, and the terms on the right-hand side represent the effects of advection and mixing, which is a sink for variance.

b. Mixedness

A complementary property to the salinity variance is the mixedness m. We define the mixedness as

$$m = (s_{\text{max}} - s)(s - s_{\text{min}}), \tag{5}$$

where s_{max} and s_{min} are the maximum and minimum salinities, respectively. For an estuary it can be assumed that $s_{\text{min}} = 0$ since the river input is freshwater. Therefore we have

$$m = s_{\text{max}} s - s^2. \tag{6}$$

Figure 1 shows graphically how mixedness and salinity variance are related for an example scenario. The mixedness is zero for the two endmembers s_{max} and s_{min} , and has its peak at $s_{\text{max}}/2$, while the variance is zero at the mean salinity \bar{s} and increases away from the mean. Because we will generally not have $s_{\text{max}}/2 = \bar{s}$, it may not be possible to achieve the maximum mixedness $s_{\text{max}}^2/4$ everywhere, even in a volume that is fully homogenized where the salinity variance is zero. In the

Salish Sea, similarly to Fig. 1, the mean salinity is closer to the oceanic salinity than to the freshwater rivers. If we consider truly "mixed" water to have salinity \bar{s} , the mixedness m is not a perfect measure unless the mixing involves equal amounts of the fresh and salty endmembers. However, because the mixedness curve varies gradually around its maximum, the overall mixedness will still increase as the salinity variance decreases. By combining a salt budget with a salt-squared budget we may construct a mixedness budget:

$$\frac{d}{dt} \int_{V} m \, dV = -\int_{A} m\mathbf{u} \cdot \hat{\mathbf{n}} \, dA + 2 \int_{V} \mathbf{K} \cdot (\nabla s')^{2} dV. \tag{7}$$

Note that the last term is the same mixing term present in the salinity variance budget, except that it is positive and acts as a source of mixedness.

3. Methods

a. Model overview

The model used is a realistic simulation of the coastal waters of Oregon, Washington, and southern British Columbia called LiveOcean, created by the University of Washington Coastal Modeling Group. A description of the model and its validation can be found in MacCready et al. (2021). The model is built using the Regional Ocean Modeling System (ROMS), and uses a spherical grid in the horizontal, with grid lines along constant latitudes and longitudes. The cell dimensions vary from 500 m in the Salish Sea to 1500 m offshore. The model has 30 s-coordinate terrain-following vertical layers, which are more closely spaced near the surface and sea floor to better resolve boundary effects. The time step is 40 s.

For external forcing, the model includes 45 rivers, with data from USGS and Environment Canada flow gauges. Atmospheric forcing is provided by a regional Weather Research

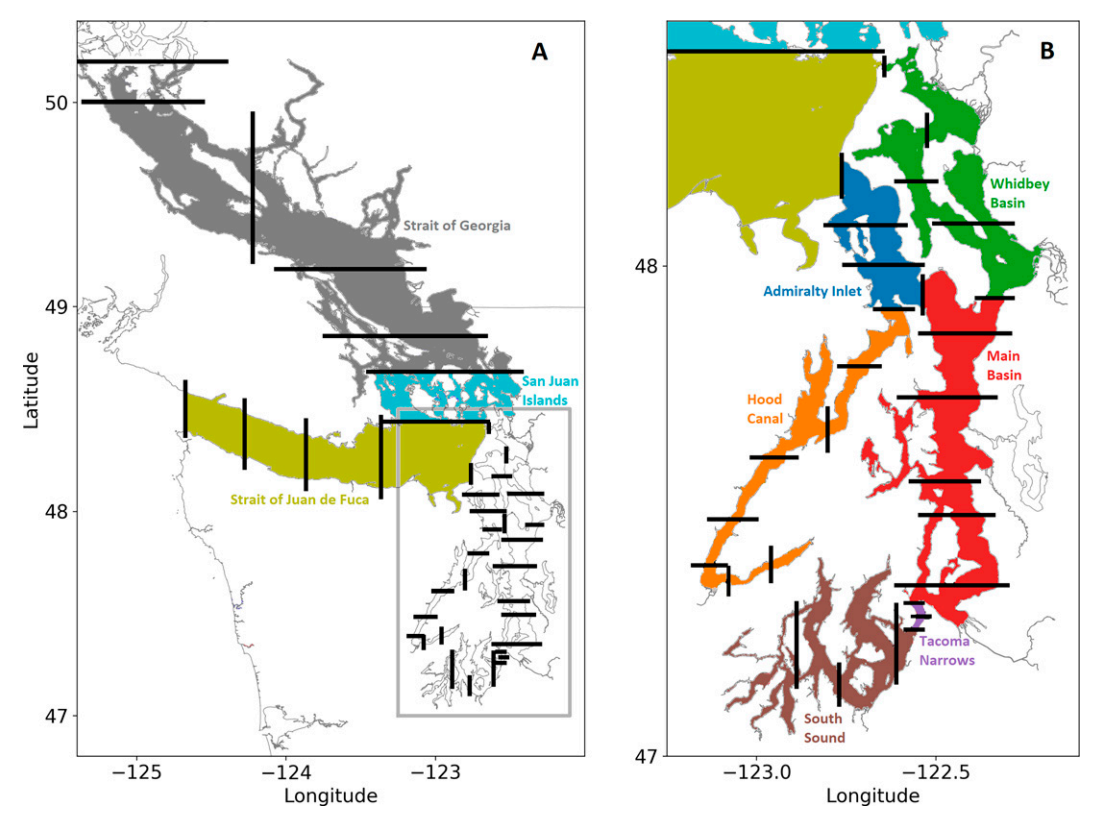


FIG. 2. (a) Map showing the nine basins used in this project, with (b) inset map of Puget Sound. The bold black lines are the sections dividing the smaller volume segments used in MacCready et al. (2021). Adapted from MacCready et al. (2021).

and Forecasting (WRF) Model. The open ocean boundary is forced by the Hybrid Coordinate Ocean Model (HYCOM) and eight tidal constituents from the TPXO tide model. We use the output of a 3-yr hindcast for 2017–19, with history files which record the instantaneous model fields at hourly intervals.

b. Basins

We divide the Salish Sea into nine different basins: South Sound, Tacoma Narrows, Main Basin, Hood Canal, Whidbey Basin, Admiralty Inlet, the San Juan Islands, the Strait of Juan de Fuca, and the Strait of Georgia. Salinity variance budgets can be made for any of these individual basins, which requires calculating *s'* using the mean salinity within the individual basin volume. We will also occasionally consider Puget Sound, which consists of the first six basins listed, as well as the Salish Sea as a whole. To divide the model domain into these basins we use the same framework as MacCready et al. (2021), but group together several of the smaller volume segments in each basin, as shown in Fig. 2.

c. Diagnostic budgets

In the LiveOcean model, we can choose to save the ROMS diagnostics and averages files at hourly intervals, in addition to the hourly history (snapshot) files. The averages files, given on the half-hour, record the average of the model fields over every time step within the hour. The diagnostics files record

information about how the model behaves internally. The diagnostics fields contain the rates of change of water properties in each cell due to various processes resolved in the model. These rates of change are an average over the hour, quoted on the half-hour.

Starting with a salt budget for a single cell made up of diagnostics terms, we follow a procedure similar to section 2a to construct an exact salinity variance budget with a vanishingly small residual. Details of the derivation can be found in the appendix. The diagnostics salinity variance budget equation is

$$\int_{V} 2s' \left[\text{salt_rate} - \frac{s}{\delta} \frac{\partial \delta}{\partial t} \right] dV$$

$$= \int_{V} 2s' \left[\text{salt_xavd} + \text{salt_yavd} + \left(\text{salt_vavd} - \frac{s}{\delta} \frac{\partial \delta}{\partial t} \right) \right] dV$$

$$+ \int_{V} 2s' \left[\text{salt_hdiff} + \text{salt_vdiff} \right] dV, \tag{8}$$

where the left-hand side represents storage, the first term on the right-hand side represents advection, and the second term on the right-hand side represents mixing. This is of the same form as the salinity variance budget given in Eq. (4), although here we calculate the advection term using a volume integral instead of invoking the Reynolds transport theorem to calculate the advective transport through the open boundaries.

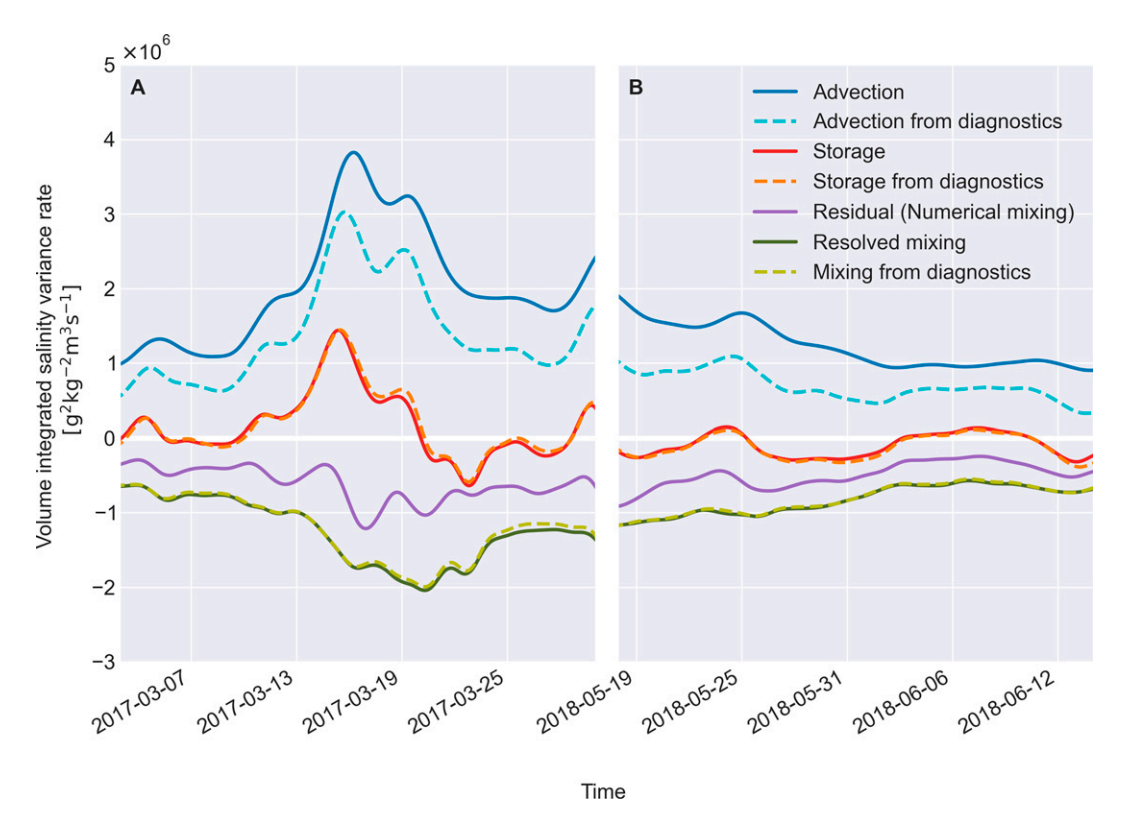


FIG. 3. Comparison of terms from history and diagnostic budgets for Puget Sound in (a) March 2017 and (b) May/June 2018. The history budgets have a residual due to numerical mixing which is the cause of the large difference between the history and diagnostic advection terms.

Salt_xavd, salt_yavd, and salt_vavd are diagnostics fields that give the rates of change due to advection in the x, y, and z directions, respectively, and salt_hdiff and salt_vdiff are diagnostics that give the rates of change due to horizontal and vertical diffusion, respectively. Salt_rate is the total rate of change in the salt content of the model cell, and δ is the cell thickness, which changes over time.

The advantage of using the diagnostics to form salinity variance budgets is that the budget closes exactly on a cell-by-cell basis, so a volume-integrated budget will close with no residual. Figure 3 shows an example of diagnostic budgets for Puget Sound (alongside budgets constructed from the history files which will be covered in section 3d). The diagnostic budgets have been tidally averaged using a Godin filter (Godin 1972; Walters and Heston 1982). The advection term is positive since river and ocean inflow bring salinity variance into the estuary, while the outflow of mixed water removes a small amount of variance. Most of the variance that is imported through advection is destroyed by mixing.

It is important to note that the diagnostics budgets do not include the effects of numerical mixing, consistent with the numerical mixing method outlined in Burchard and Rennau (2008). Nonetheless, the diagnostic budgets are useful for validating salinity variance budgets calculated from the history files alone by comparing their storage, horizontal mixing, and vertical mixing terms.

d. Three-year salinity variance budgets

To make salinity variance budgets over the three years of our model hindcast, we need to estimate the storage, mixing, and advection terms from the history files. The storage term can be estimated by calculating the mean salinity for the chosen volume at every hour to create a time series of total salinity variance in the basin. We then use centered differencing to find the rate of change, and filter the time series with a Godin filter. To estimate the mixing term, we calculate the resolved mixing using Eq. (4):

$$M_{\text{resolved}} = 2 \int_{V} \mathbf{K} \cdot (\nabla s')^{2} dV.$$
 (9)

We can split the resolved mixing into vertical and horizontal components, M_V and M_H :

$$M_V = 2 \int_V K_V \left(\frac{ds}{dz}\right)^2 dV,\tag{10}$$

$$M_H = 2 \int_V K_H \left[\left(\frac{ds}{dx} \right)^2 + \left(\frac{ds}{dy} \right)^2 \right] dV, \tag{11}$$

where K_V is the vertical eddy diffusivity, and K_H is the horizontal eddy diffusivity, which is a constant (2.0 m² s⁻¹). To calculate the horizontal gradients, we use simple centered

differencing along the terrain-following layer, neglecting layer height variations. By comparing our results to the diagnostic budgets, we determined that applying a correction to account for the slope of the layer resulted in worse performance, likely due to discretization errors.

The last term that we need to estimate is the advection term. We use the TEF (MacCready 2011) to find the tidally averaged advection as a sum of three terms: a river term, and inflowing and outflowing terms representing an equivalent two-layer flow at the open boundaries. The TEF method decomposes the flow through a section in salinity coordinates into an equivalent two-layer exchange flow $Q_{\rm in}$ and $Q_{\rm out}$ (MacCready 2011). To find the TEF, flow through a section is binned according to its salinity class, tidally averaged, and then grouped into inflowing and outflowing layers. We use 1000 salinity classes with the dividing salinity method described in Lorenz et al. (2019), which is more numerically robust, to find $Q_{\rm in}$ and $Q_{\rm out}$ at the bounding sections of each basin. The flux-weighted salinities of the inflow and outflow, denoted by s_{in} and s_{out} , respectively, can then be found from the salt flux in each layer. We can also find the flux-weighted $s_{\rm in}^2$ and $s_{\rm out}^2$ at each section. We then use these known quantities to efficiently calculate the flux-weighted salinity variance at each section:

$$s_{\rm in}^{\prime 2} = s_{\rm in}^2 - 2s_{\rm in}\bar{s} + \bar{s}^2, \tag{12}$$

$$s_{\text{out}}^{\prime 2} = s_{\text{out}}^2 - 2s_{\text{out}} \overline{s} + \overline{s}^2. \tag{13}$$

This is advantageous because performing the TEF extractions is computationally expensive. We want to create salinity variance budgets for eleven individual basins, each with a different mean salinity. This method allows us to find the $s_{\rm in}^{\prime 2}$ and $s_{\rm out}^{\prime 2}$ for a given mean salinity without actually extracting the fluxes of $s_{\rm in}^{\prime 2}$ through each section. We can then use the $s_{\rm in}^{\prime 2}$ and $s_{\rm out}^{\prime 2}$ to form the advection term for a salinity variance budget:

$$-\int_{A} s'^2 \mathbf{u} \cdot \hat{\mathbf{n}} \, dA = Q_r \overline{s}^2 + Q_{\text{in}} s'_{\text{in}}^2 + Q_{\text{out}} s'_{\text{out}}^2, \tag{14}$$

where Q_r is the river flow and Q_{out} is defined as being negative. This is similar to the formulation given in Eq. (33) of Burchard et al. (2019), except that the covariance between the river flow and the mean salinity is not included.

We can categorize the basins as "enclosed" or "non-enclosed" based on whether the flow at all of its bounding sections is in the same direction. For the enclosed basins, such as Whidbey Basin, flow into the basin $(Q_{\rm in})$ is in the "landward" direction at all openings. For enclosed basins with more than one bounding section we can combine the $Q_{\rm in}$ or $Q_{\rm out}$ from openings and find a single combined flux-weighted value of $s_{\rm in}^{\prime 2}$ and $s_{\rm out}^{\prime 2}$ for the basin. For the non-enclosed basins, such as Tacoma Narrows, flow into the basin is "landward" at some openings and "seaward" at others. In this case, the TEF variables must be kept separate for each boundary. In such cases, calculating a combined value for $s_{\rm in}^{\prime 2}$ or $s_{\rm out}^{\prime 2}$ yields little physical insight.

Figure 3 shows the three terms (storage, mixing and advection) calculated from the diagnostics and history files for Puget Sound

for the two months where the diagnostics are available. As expected, the advection term is much larger in the history budgets due to the effects of numerical mixing. The residual from the history budgets, shown in purple, is an estimate of the numerical mixing. As shown in Fig. 3, the resolved mixing and storage terms calculated using the history files are very similar to the mixing and storage from the diagnostic budgets. We have also previously used the history files to construct volume and salt budgets (not shown) that close with a small residual, which implies that our advection calculation method is sound. Therefore, we can be reasonably confident that the residual is primarily due to numerical mixing and not other errors.

Now we can use the history budget method to construct salinity variance budgets for the full three years 2017-19. The salinity variance budget for the Salish Sea using the history budget method is shown in Fig. 4, where the resolved mixing and estimated numerical mixing have been grouped together. We refer to the sum of the resolved and numerical mixing as the total mixing. Figure 4 also shows the breakdown of the total advection into its TEF components. Even though the river flow is much smaller than the exchange flow, the river contribution dominates the advection term in the salinity variance budget because the fresh river water has very high variance. The inflowing exchange flow term is slightly larger than the outflowing term, even though Q_{in} and Q_{out} have very similar magnitudes, because s_{out} is close to \bar{s} . Figure 4c shows the breakdown of the total mixing into resolved and numerical mixing, along with the horizontal contribution to the resolved mixing. We also create salinity variance budgets for all nine smaller basins shown in Fig. 2, as well as Puget Sound, and the mixing terms from these budgets will be used to answer our research questions.

e. Mixedness transport

Similarly to section 3d, we can write the mixedness budget in terms of the TEF variables:

$$\frac{d}{dt} \int_{V} m dV = Q_{\text{in}} m_{\text{in}} + Q_{\text{out}} m_{\text{out}} + 2 \int_{V} \mathbf{K} \cdot (\nabla s')^{2} dV, \quad (15)$$

where there is no contribution from the freshwater rivers which have m = 0. The inflowing and outflowing mixedness $m_{\rm in}$ and $m_{\rm out}$ are calculated as

$$m_{\rm in} = (s_{\rm in})(s_{\rm max}) - s_{\rm in}^2,$$
 (16)

$$m_{\text{out}} = (s_{\text{out}})(s_{\text{max}}) - s_{\text{out}}^2, \tag{17}$$

where we use the highest $s_{\rm in}$ in the 3-yr time series as $s_{\rm max}$. It is necessary to use $s_{\rm out}^2$ rather than $(s_{\rm out})^2$ to obtain the correct flux-weighted mixedness.

To study when mixed water is expelled from the estuary, we use the outflowing mixedness transport $Q_{\rm out}m_{\rm out}$. We calculate time series of outflowing mixedness for six enclosed basins: the entire Salish Sea, Puget Sound, South Sound, Hood Canal, Whidbey Basin, and the Strait of Georgia. Since the remaining basins do not have a well-defined $Q_{\rm out}$, $s_{\rm out}$, and $s_{\rm out}^2$

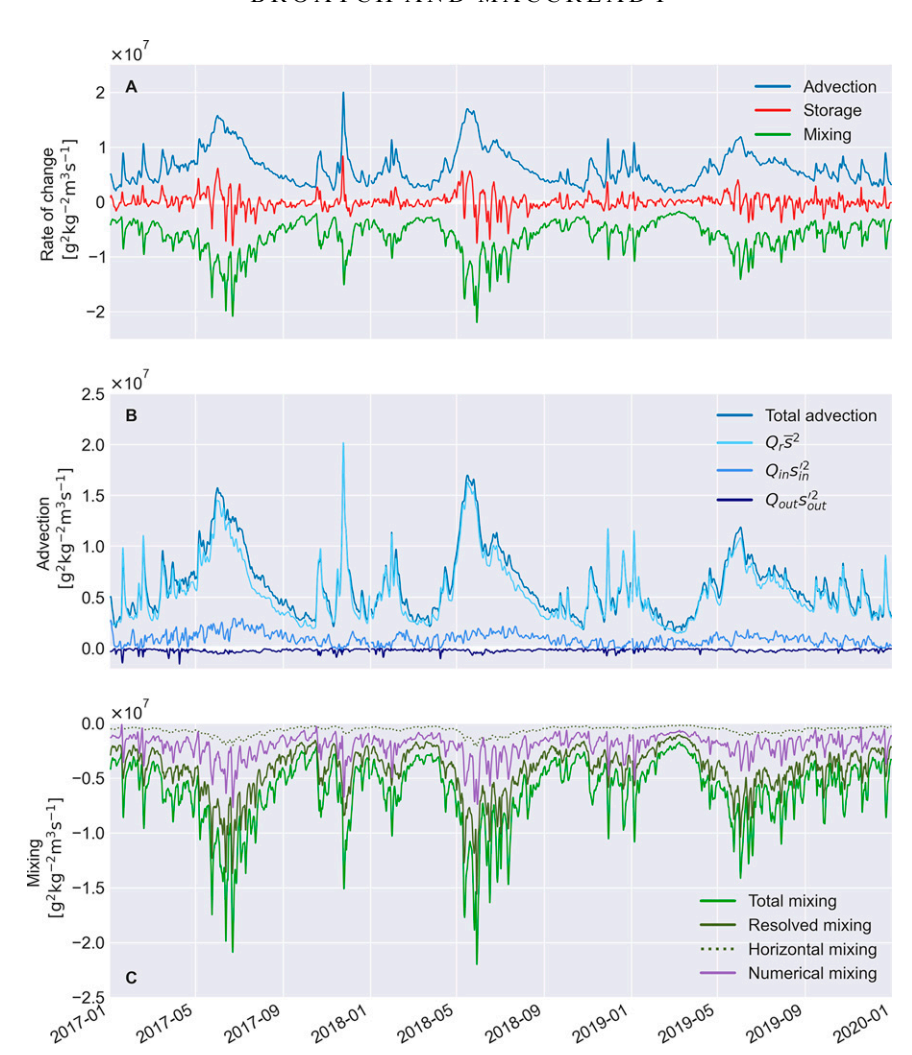


FIG. 4. (a) Salinity variance budgets for 2017–19 calculated from history files in the Salish Sea. This budget closes by construction since the residual (estimated numerical mixing) is grouped into the mixing term. (b) Breakdown of the advection term from the Salish Sea salinity variance budget into river, inflow, and outflow components. (c) Breakdown of the mixing term from the Salish Sea salinity variance budget. The total mixing is the sum of the resolved and numerical mixing. The horizontal mixing is a component of the resolved mixing.

(see section 3d), they are excluded from this portion of the analysis.

f. Forcing factors

To study the timing of mixing, we look at the correlation with three forcing factors: rivers, tides, and winds. For the rivers, we use the total river flow Q_r from all rivers entering a given segment. Since the forcing files for the model only have a single river flow value per day, the total river flow is smoothed with the Godin filter, consistent with the other budget terms and forcing factors. We use the surface current and surface wind stress to calculate the energy input from winds (Yu et al. 2018):

$$P_{\text{wind}} = \int_{A} \boldsymbol{\tau}_{s} \cdot \mathbf{u}_{s} dA, \tag{18}$$

where τ_s is the surface wind stress and \mathbf{u}_s is the surface current

Because the quantities required are on different coordinates of the model grid, we interpolate the fields to the center of each cell using simple averaging. The area integral over the surface of the basin gives a rate of wind energy input to the ocean in watts. The time series of wind forcing is then filtered using the Godin filter. For the tides, we use the same method with the bottom velocities and bottom stress to calculate the energy dissipation due to bottom drag. Although the velocity right at the bottom is zero due to the no-slip condition, the stress and velocity in the bottom model cell can be used to calculate the energy dissipation in a layer just above the bottom. This is appropriate because we are using the tidally averaged energy dissipation near the bottom as a timekeeper for the spring—neap cycle and not as part of an energy budget.

TABLE 1. Average values of numerical mixing as a percentage of the total mixing in each basin for 2017–19.

Basin	Numerical mixing (% of total mixing
Tacoma Narrows	73.3
Hood Canal	59.6
South Sound	57.2
San Juan Islands	50.7
Admiralty Inlet	48.8
Strait of Juan de Fuca	42.2
Main Basin	37.5
Whidbey Basin	31.3
Strait of Georgia	27.5
Puget Sound	36.6
Salish Sea	32.4

To study the correlation between the forcing factors and the mixing or mixedness transport, we use a lagged correlation (up to 15 days lag, in 1-h increments) to find the maximum Pearson's correlation coefficient *r*.

4. Results and discussion

a. Numerical mixing

The different contributions to the total mixing term are shown in Fig. 4 for the Salish Sea. Although the total resolved and numerical mixing balances the salinity variance budget, any conclusions drawn from the model output rely on whether the simulated total mixing is a good representation of the mixing that occurs in the real ocean. It is challenging to make observations that can be used to validate the mixing in the model. However, there are other ways to evaluate the impact of numerical mixing on our results.

First, we can examine the size of the numerical mixing in comparison with the resolved mixing, and whether it dominates the total mixing. On average, about one-third of the total mixing in the Salish Sea is due to numerical mixing in the model. This is reasonable for a realistic numerical model of a complex estuary. In Li et al. (2018), numerical mixing accounts for approximately one-third of the total mixing in their model of the Changjiang estuary. In contrast, models of

estuaries with simpler geometries, such as the idealized model used in MacCready et al. (2018) or the Hudson river model used in Wang et al. (2017), have small, but nonnegligible, numerical mixing. Ralston et al. (2017) found that approximately half of the mixing was numerical in a model of the Connecticut River estuary, although they used the Finite Volume Community Ocean Model (FVCOM) with an unstructured grid.

Because numerical mixing is a model artifact caused by discretization errors in the advection scheme, it will not necessarily have the same spatial structure as the resolved mixing. Therefore, we also want to know whether the proportion of numerical mixing is similar across the different basins in the Salish Sea. Table 1 shows the average percentage of the total mixing that is due to numerical mixing in each basin. We can see that there is a wide variation, with the numerical mixing accounting for an average of 27%–73% of the total mixing, depending on the location. The high numerical mixing in Tacoma Narrows is likely because it is not well resolved, being only two cells wide in some places. On the other hand, the high proportion of numerical mixing in Hood Canal and South Sound, which are generally more stagnant, may simply be because there is not much resolved mixing in these basins.

To examine whether the numerical mixing has temporal behavior similar to the resolved mixing, we use a linear regression of the numerical mixing against resolved mixing to see whether the numerical mixing stays at a constant proportion of the total mixing in each basin. The numerical mixing is most highly correlated in time with the resolved mixing in the San Juan Islands ($r^2 = 0.97$) while the lowest correlation by a significant margin is in Whidbey Basin ($r^2 = 0.51$). Overall, the numerical mixing is well correlated temporally with the resolved mixing in most basins, with $r^2 = 0.76$ for the Salish Sea as a whole. The numerical mixing occurs at roughly the same place and time as the resolved mixing, and therefore should not adversely affect the analysis of mixing location and timing presented in the following sections.

b. Geographic distribution of mixing

To examine where mixed water is created in the Salish Sea, we divide our study region into nine basins, as shown in

TABLE 2. Average values of the volume-normalized total mixing, integrated total mixing, and horizontal mixing as a percentage of the resolved mixing, in each basin for 2017–19. The nominal volume (with sea surface height $\zeta = 0$) is also given. The largest value in each column (excluding the totals for Puget Sound and the Salish Sea) is bolded.

Basin	Volume-normalized total mixing (g ² kg ⁻² s ⁻¹)	Integrated total mixing (g ² kg ⁻² m ³ s ⁻¹)	Horizontal mixing (% of resolved mixing)	Volume (m ³)
Whidbey Basin	2.4×10^{-5}	6.5×10^{5}	14.0	2.7×10^{10}
Tacoma Narrows	5.5×10^{-6}	2.3×10^{3}	5.4	4.2×10^{8}
San Juan Islands	4.3×10^{-6}	3.1×10^{5}	18.4	7.2×10^{10}
Admiralty Inlet	4.1×10^{-6}	7.1×10^4	20.1	1.7×10^{10}
Main Basin	3.1×10^{-6}	2.6×10^{5}	14.5	8.5×10^{10}
South Sound	3.1×10^{-6}	4.8×10^{4}	4.1	1.6×10^{10}
Strait of Georgia	3.0×10^{-6}	4.0×10^{6}	13.5	1.3×10^{12}
Hood Canal	2.9×10^{-6}	7.2×10^4	17.3	2.5×10^{10}
Strait of Juan de Fuca	2.1×10^{-6}	9.0×10^{5}	22.9	4.4×10^{11}
Puget Sound	6.5×10^{-6}	1.1×10^{6}	14.3	1.7×10^{11}
Salish Sea	3.1×10^{-6}	6.3×10^{6}	14.9	2.0×10^{12}

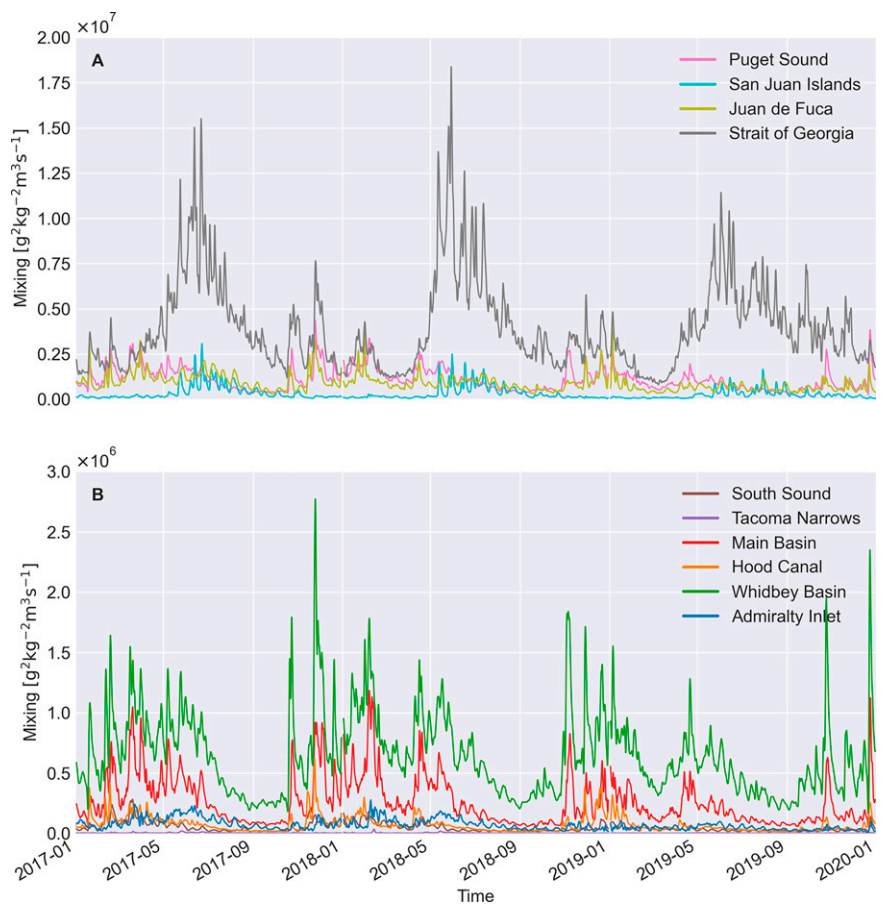


FIG. 5. (a) Mixing in the four major basins of the Salish Sea for 2017–19, with all the Puget Sound basins grouped together into the pink line, and (b) the breakdown of mixing in each basin of Puget Sound.

Fig. 2. The average mixing in each basin for 2017–19 is shown in Table 2. To start, we group the six smaller basins within Puget Sound together, leaving four "major basins" (Strait of Georgia, Strait of Juan de Fuca, San Juan Islands, and Puget Sound). Figure 5a shows the mixing contributions of the four

major basins. The largest contribution, with an average of about $4\times10^6~g^2~kg^{-2}~m^3~s^{-1}$, is from the Strait of Georgia, which is also the largest basin, with about two-thirds of the overall volume of the Salish Sea. Note that the total mixing in the Salish Sea is $6.3\times10^6~g^2~kg^{-2}~m^3~s^{-1}$, so the mixing in the

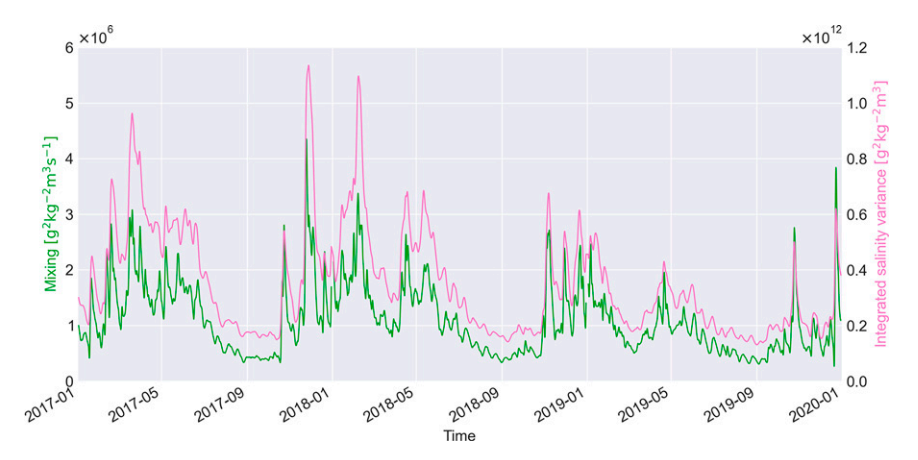


FIG. 6. Total mixing and reservoir of salinity variance in Puget Sound for 2017–19.

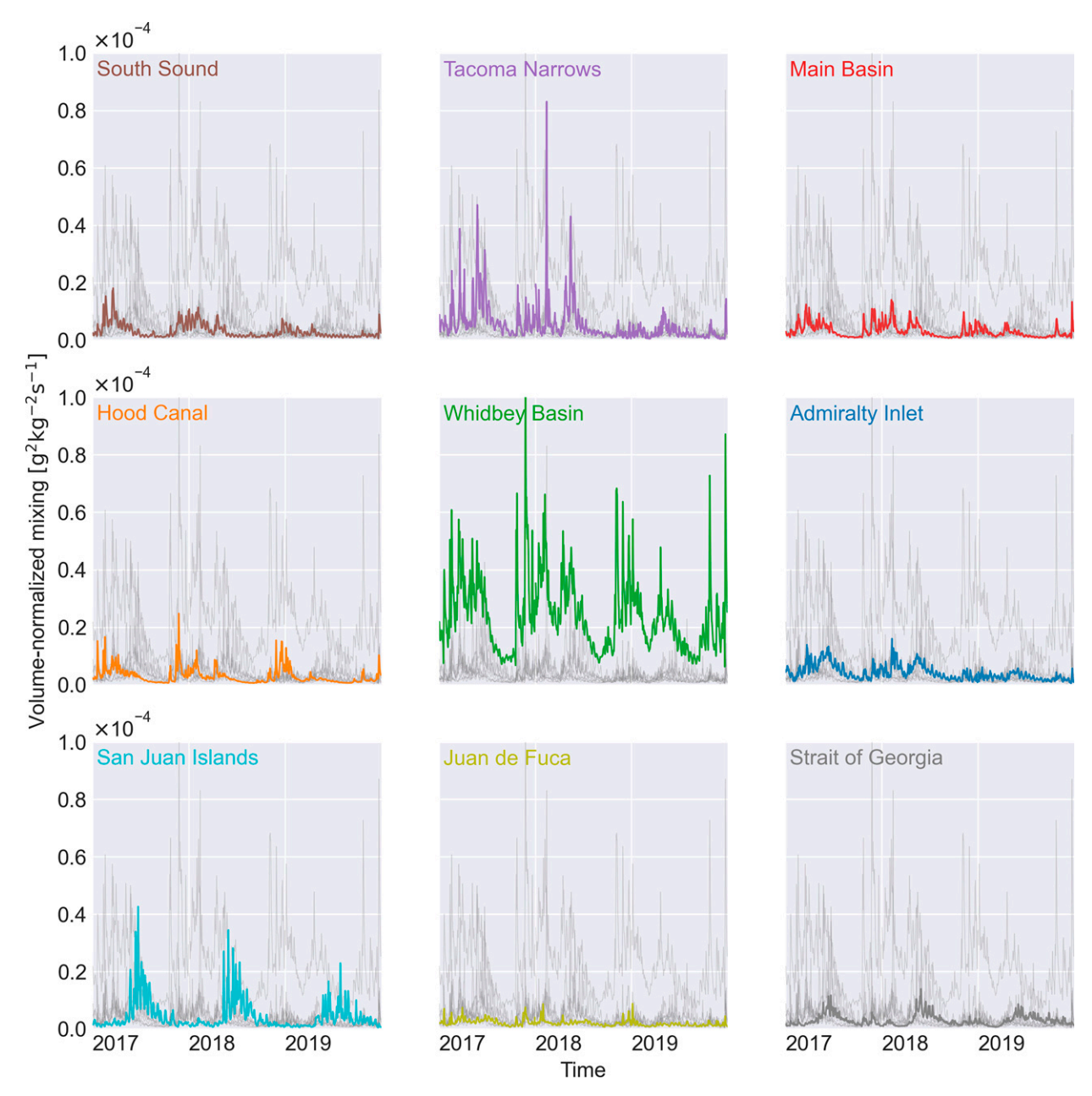


FIG. 7. Volume-normalized total mixing in each basin for 2017–19. The scale is the same in each subplot and the thin gray lines show the volume-normalized total mixing in the other basins for ease of comparison.

Strait of Georgia is approximately proportional to its volume. The Strait of Juan de Fuca and Puget Sound have similarly sized contributions of around $1\times 10^6~{\rm g^2~kg^{-2}~m^3~s^{-1}}$. The San Juan Islands have strongly seasonal mixing, with low mixing on the order of $1\times 10^5~{\rm g^2~kg^{-2}~m^3~s^{-1}}$ during the winter, but often exceeding the mixing of the Strait of Juan de Fuca or Puget Sound during the summer months.

To provide context for these mixing rates, consider Fig. 6, which shows a time series of the salinity variance reservoir and mixing in Puget Sound. The average variance is 3.5×10^{11} g² kg⁻² m³. With an average mixing rate for Puget

Sound of 1.1×10^6 g² kg⁻² m³ s⁻¹, the reservoir divided by the rate gives a time scale of ~3.7 days for all salinity variance to be mixed away.

Taking a closer look at the mixing within Puget Sound (Fig. 5b), we see that Whidbey Basin makes the largest contribution with over half of the total mixing in the Sound. Whidbey Basin is one of the shallower basins in Puget Sound and has large river inflow (the Skagit River accounts for approximately half of the river flow into Puget Sound). This large input of freshwater leads means that there is more salinity variance (as horizontal gradients and high stratification) available to be

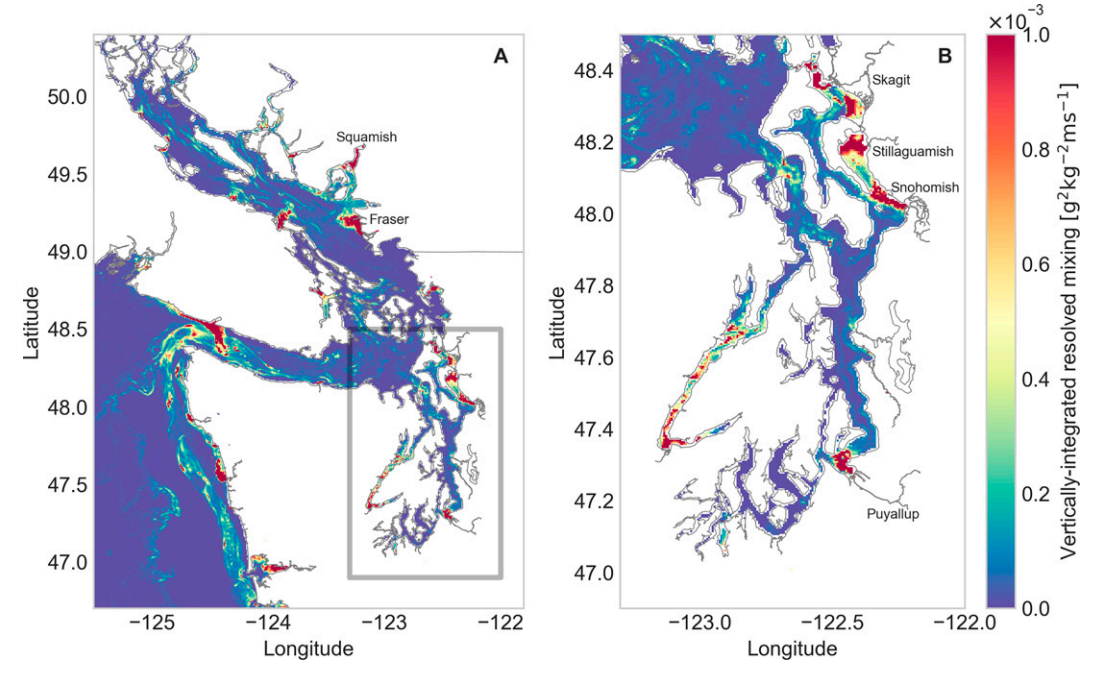


FIG. 8. Map of vertically integrated resolved mixing per unit horizontal area at 1900 UTC 19 Jan 2017 in (a) the Salish Sea and (b) Puget Sound. Selected rivers are labeled. Note that the mixing is highly concentrated at the river mouths.

destroyed by mixing. Main Basin also has a significant contribution, primarily due to its large size.

Figure 5 concerned only the integrated total mixing. Alternatively, we may consider the volume-normalized total mixing in each basin, as shown in Fig. 7. Here we can clearly see that Whidbey Basin has the most intense mixing. Other areas of intense mixing are Tacoma Narrows and the San Juan Islands. The weaker mixing in 2019 is associated with lower-than-average river flows. The 3-yr average of volume-normalized total mixing in each basin is shown in Table 2.

Puget Sound has historically been considered as a network of quiescent basins connected by highly energetic sills where strong mixing occurs (Cokelet and Stewart 1985; Ebbesmeyer et al. 1988). In contrast, the combined mixing that occurs at Tacoma Narrows and Admiralty Inlet in our results only accounts for about 6.6% of the mixing in Puget Sound. The mixing is also not significantly more intense at these sills. Aside from Whidbey Basin, all the basins within Puget Sound have average volume-normalized total mixing within the same order of magnitude. Although Tacoma Narrows and Admiralty Inlet have the strongest mixing after Whidbey Basin, their volume-normalized mixing rates are still less than double that of Hood Canal, which has the weakest mixing in Puget Sound.

On a finer scale, we can look at a map of resolved mixing in the Salish Sea. Because we have estimated the numerical mixing as the residual of the salinity variance budget for an entire basin, we cannot determine the amount of total mixing in each cell or water column. Figure 8 shows an example of the vertically integrated resolved mixing per unit horizontal area. Within each basin, the mixing is primarily concentrated at the river mouths, which are sources of high-variance water.

As described in section 3d, horizontal mixing is not negligible in the model. In assessing where mixed water is produced, a related question is whether the breakdown between vertical and horizontal mixing is consistent across the various basins. Table 2 shows the percentage of the resolved mixing that is due to horizontal mixing in each basin. Overall, horizontal mixing accounts for ~15% of the resolved mixing in the Salish Sea, with values as low as 4%–5% in South Sound and Tacoma Narrows, and as high as 23% in the Strait of Juan de Fuca. The K_H is constant in the model (2.0 m² s⁻¹), so the amount of horizontal mixing depends primarily on how strong the horizontal salinity gradients are.

c. Correlation of mixing and forcing factors

To ascertain when mixed water is produced in the Salish Sea, we look at the correlation of mixing with various forcing factors. In Fig. 5 we can see that the various basins have different timing for their peaks in mixing. Puget Sound and the Strait of Juan de Fuca have their peak in mixing during the winter, while the Strait of Georgia and San Juan Islands peak later in the spring. To study the timing of mixing in the Salish Sea we consider three different external forcings as described in section 3f. Figure 9 shows the river flow, spring-neap cycle, and wind time series overlaid on the total mixing in the Salish Sea. It is immediately apparent that the mixing most closely follows the river flow curve. Note that there is a declining trend in the river flow over the three years studied. Figure 10 shows the correlation coefficient r from a lagged correlation of the mixing term with the three forcing factors for each basin. The rivers are the dominant forcing factor and positively correlated with the mixing magnitude in most basins, with

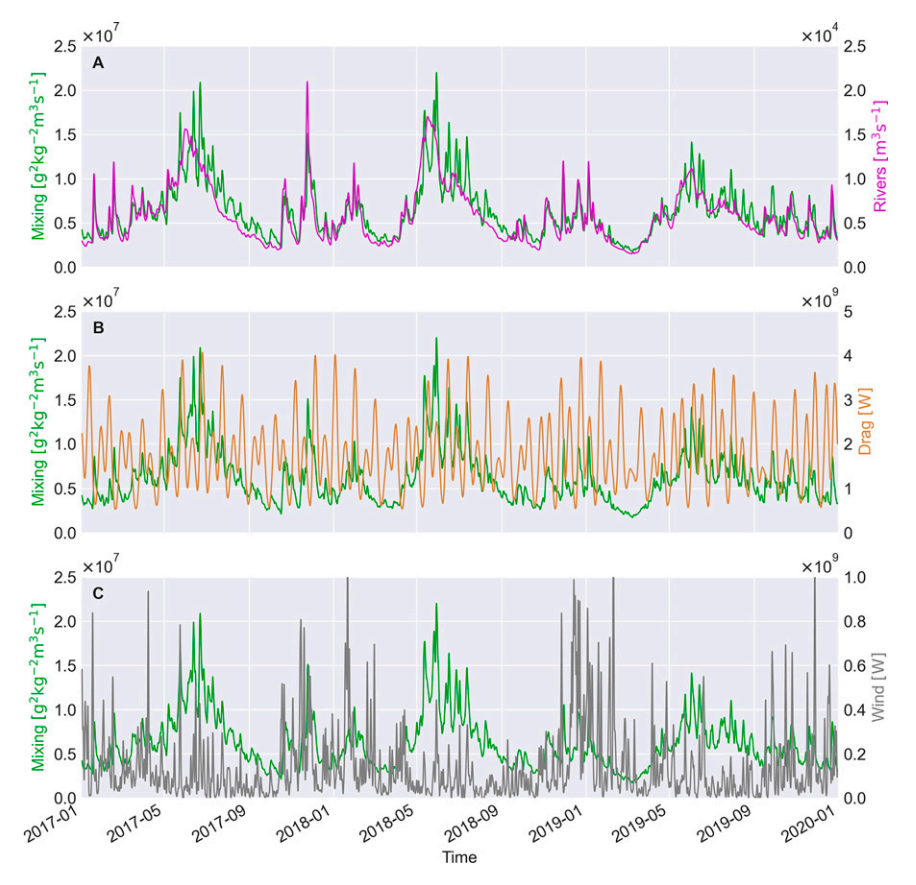


FIG. 9. Time series of mixing in the Salish Sea for 2017–19 plotted with three different forcing factors: (a) total river flow, (b) energy dissipation due to bottom drag which represents the spring–neap cycle, and (c) energy input from winds. Note that the mixing most closely follows the shape of the river flow time series.

winds and tides being of secondary importance. The lag between the river flow and mixing ranges from 11 h in the Strait of Juan de Fuca to 39 h in the Strait of Georgia. Tacoma Narrows and Admiralty Inlet do not have rivers entering them directly. The correlation coefficients of mixing with rivers entering basins landward of Tacoma Narrows and Admiralty Inlet are 0.41 and 0.55, respectively. Similarly, the correlation of mixing with rivers in the San Juan Islands actually has a small negative correlation. However, only the Samish River enters the San Juan Islands segment directly, but mixing in the San Juan Islands is influenced by the Fraser River flow which enters the Strait of Georgia. The maximum correlation of the San Juan Islands mixing with the rivers entering the Strait of Georgia is 0.69.

We have determined that mixing is highly correlated with river flow. To answer our question of when mixed water is created, we need to know what creates the different patterns of river flow in each basin. The overall annual cycle of the river flow depends on what type of watershed it drains (Casola et al. 2005; Lee and Hamlet 2011). In snow-dominant watersheds, snow accumulates in the watershed over the winter and peak flow is during the spring when snow melts. In rain-dominant watersheds, peak flow is during the winter due

to heavy precipitation. Mixed rain and snow watersheds generally have two peaks, one in the winter and one in the spring. This explains why the Strait of Georgia and San Juan Islands have their mixing peak in the spring, since they are most affected by the Fraser River, which has a snow-dominant watershed. The rivers entering the Strait of Juan de Fuca and Puget Sound mostly have rain-dominated or mixed watersheds, which is why they have a flatter mixing peak across the winter and spring. Streamflow patterns in the Salish Sea and Puget Sound are predicted to change in the future, as climate change alters the size of snowpacks and how rapidly they melt, and watersheds transition toward more rain-dominated regimes (Casola et al. 2005; Lee and Hamlet 2011). Therefore, the timing of mixing in the Salish Sea will likely change in the future.

The lack of influence of the spring-neap cycle on the timing of mixing is in contrast to previous studies such as Wang et al. (2017), Li et al. (2018), MacCready et al. (2018), and Wang and Geyer (2018), where a pronounced spring-neap effect was observed. However, all of these studies except Li et al. (2018) used a constant river flow in their model setup, and a dependence of mixing on river flow was found in Wang and Geyer (2018) in their experiments testing varying levels of



FIG. 10. Radar plots showing the correlation coefficient |r| from a lagged correlation between the mixing and forcing factors in each basin. The + or - sign next to the name of the forcing factor indicates whether the correlation is positive or negative. Note that Admiralty Inlet and Tacoma Narrows do not have any rivers entering them directly, so the correlation with the landward rivers is shown instead. The San Juan Islands have only one river, the Samish River, entering directly.

constant river discharge. The river flow entering the Salish Sea, which imports high-variance water into the estuary, varies drastically throughout the year. Although the mixing is provided primarily by tides, the total amount of mixing is

controlled by how much variance is available to be destroyed rather than by the smaller fluctuations in the strength of the tides. This can also be seen in Fig. 6, where the mixing rate curve closely follows the reservoir of integrated salinity

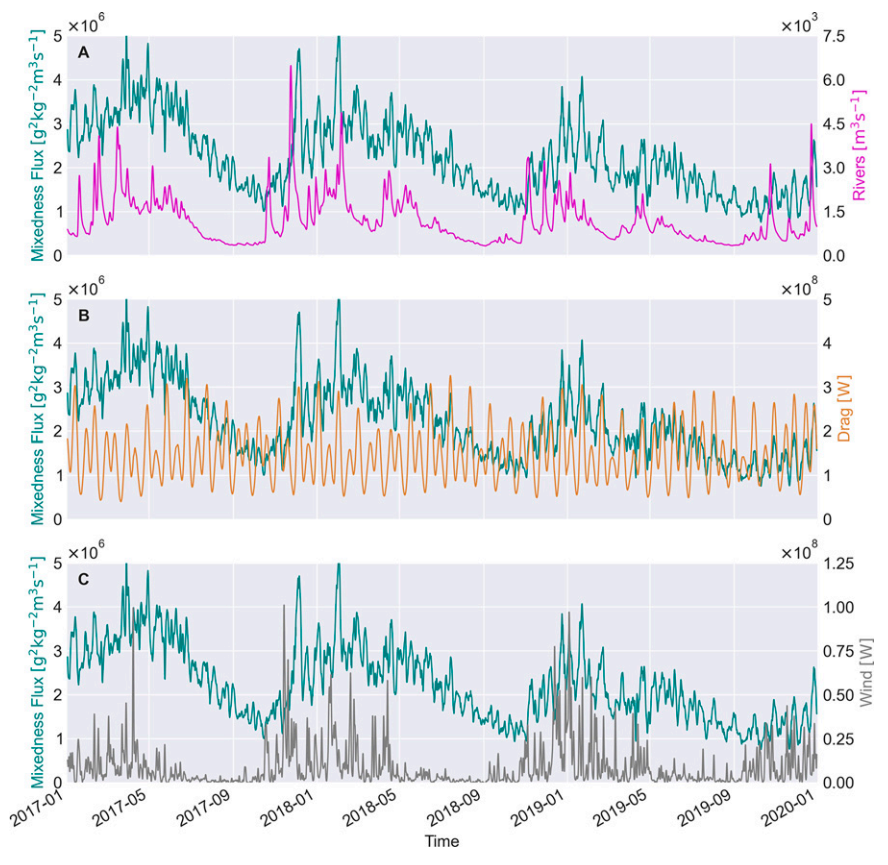


FIG. 11. Time series of outflowing mixedness transport for Puget Sound for 2017–19 plotted with three different forcing factors: (a) total river flow, (b) energy dissipation due to bottom drag which represents the spring–neap cycle, and (c) energy input from winds.

variance. The other estuaries previously studied generally have lower mean salinities than the Salish Sea, such that advection of salinity variance through the ocean boundaries plays a more significant role.

d. Removal of mixed water from the estuary

To discover when mixed water is removed from the estuary, we look at the correlation of the outflowing mixedness transport $Q_{\text{out}}m_{\text{out}}$ with the same three forcing factors used in section 4c. Note that for this section we only consider the enclosed basins, while excluding Tacoma Narrows, Main Basin, Admiralty Inlet, the San Juan Islands, and the Strait of Juan de Fuca. Figure 11 shows the river flow, spring-neap cycle, and wind time series overlaid on the outflowing mixedness transport for Puget Sound. Because we use the TEF salinity $s_{\rm out}$ to calculate the mixedness, the time series for the Salish Sea (not shown) is much noisier than that for Puget Sound. This is caused by the Columbia River plume entering the Salish Sea through the Strait of Juan de Fuca, which can promote reverse estuarine circulation, as described in Thomson et al. (2007) and Giddings and MacCready (2017). While the salinities for Puget Sound behave as expected, with sout always fresher than s_{in} , the Salish Sea has inversions when s_{in} is fresher than sout.

Figure 12 shows the correlation coefficients r from a lagged correlation of the three forcing factors with the outflowing mixedness transport for the enclosed basins. The rivers are the most important factor in every basin, and the coupling is generally tighter with the mixing (Fig. 10) than the mixedness transport. The lag between the river flow and mixedness transport time series is 9.9 days and 14.7 days in Puget Sound and the Salish Sea, respectively, which is much longer than the lag between the river flow and mixing (\sim 1 day). This is reasonable because mixing is concentrated at river mouths, far from the open boundaries where mixed water is expelled.

e. Long-term average mixing approximation

Finally, we want to determine how well the long-term average mixing approximation proposed in MacCready et al. (2018) can predict the mixing in the Salish Sea, and on what time scales. Figure 13 shows the total mixing M from the salinity variance budgets and the approximations $Q_r s_{\text{out}} s_{\text{in}}$ and $Q_{\text{in}} \Delta s s_{\text{in}}$ for Puget Sound. The time series are all tidally averaged and sampled hourly.

As shown, the long-term average approximation $Q_{\rm in}s_{\rm out}s_{\rm in}$ gives a good estimate of the mixing in Puget Sound, even without any additional time averaging. The root-mean-square error (RMSE) normalized by the mean mixing is 0.297. This

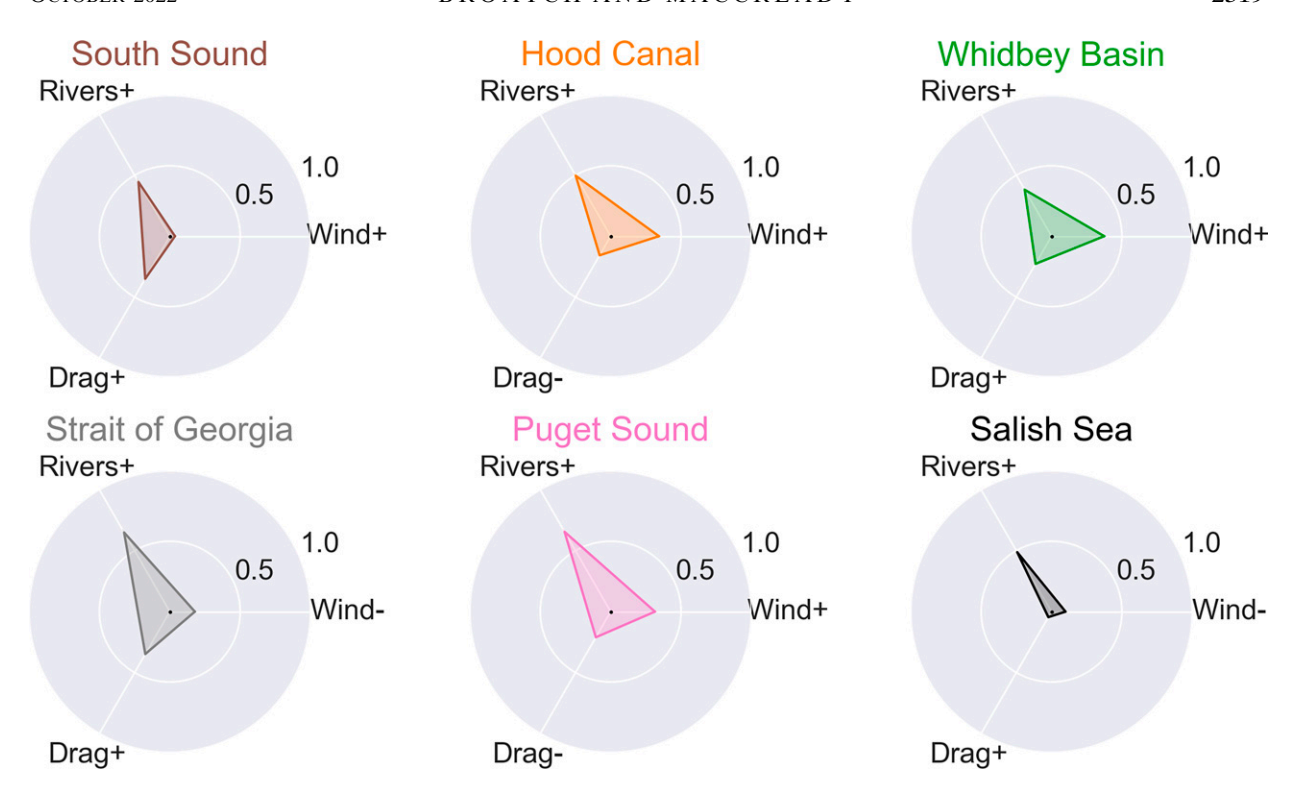


FIG. 12. Radar plots showing the correlation coefficient |r| from a lagged correlation between the outflowing mixedness transport and forcing factors in the enclosed basins. The + or - sign next to the name of the forcing factor indicates whether the correlation is positive or negative.

approximation performs similarly well in the Salish Sea as a whole, with a normalized RMSE of 0.266. Additional averaging did not significantly improve the mixing estimates. The lag between the long-term average approximation and the mixing in the history budgets is 28 h in Puget Sound and 27 h in the Salish Sea, which is on the same order of magnitude as the lag between the river flow and mixing reported in section 4c. It is somewhat surprising that an approximation that assumes timeaveraged conditions should perform so well without any temporal averaging in an environment where the river flow varies by an order of magnitude. However, most of the mixing occurs near the river mouths, and therefore the basinwide mixing reacts quickly to river discharge. Because the river flow is tightly coupled with the mixing, and the salinities s_{in} and s_{out} vary only by \sim 2 g kg⁻¹ over the year, Puget Sound and the Salish Sea are exactly the type of estuary where this type of approximation can be successfully implemented. It is particularly convenient to be able to use $M = Q_r s_{out} s_{in}$ to predict the mixing in an estuary since the formula only requires knowledge of the TEF properties on the open boundaries and the river flow, but does not require any information about the interior of the estuary. However, it should be noted that this approximation relies on the assumption that $s_{\rm in}^{\prime 2} \approx (s_{\rm in} - \bar{s})^2$ and $s_{\rm out}^{\prime 2} \approx (s_{\rm out} - \bar{s})^2$. For cases where this assumption is not valid, Burchard et al. (2019) have defined a hierarchy of mixing parameterizations with and without constancy and periodicity assumptions.

Conversely, the approximation $Q_{\rm in}\Delta ss_{\rm in}$ does not follow the mixing curve closely in Puget Sound. This is likely due to time dependence of variance storage in the system. As shown in

Fig. 13, the peaks of $Q_{\rm in}\Delta ss_{\rm in}$ align with neap tides. This is consistent with the findings of Geyer and Cannon (1982) that the gravitational circulation and stratification at Admiralty Inlet were greatest at neap tides. However, the 3-yr average of mixing in Puget Sound is 1.10×10^6 g² kg⁻² m³ s⁻¹, while $Q_r s_{\rm out} s_{\rm in}$ and $Q_{\rm in}\Delta ss_{\rm in}$ have averages of 1.12×10^6 and 1.19×10^6 g² kg⁻² m³ s⁻¹, respectively. Therefore, over a long time average, $Q_{\rm in}\Delta ss_{\rm in}$ may be used to provide a reasonable estimate of mixing in Puget Sound. Note that this approximation is not a good choice for the Salish Sea as a whole, due to the reversals in estuarine circulation discussed previously, which lead to negative values of Δs .

The salt budget in an estuary may be expressed in terms of the TEF variables:

$$\frac{d}{dt} \int_{V} s \, dV = Q_{\rm in} s_{\rm in} + Q_{\rm out} s_{\rm out}. \tag{19}$$

By substituting $Q_r = -(Q_{\rm in} + Q_{\rm out})$ and $\Delta s = s_{\rm in} - s_{\rm out}$, we may alternatively express the salt budget as

$$\frac{d}{dt} \int_{V} s \, dV = Q_{\rm in} \Delta s - Q_{r} s_{\rm out},\tag{20}$$

where $Q_{\text{in}}\Delta s$ represents the exchange flow salt transport and $Q_r s_{\text{out}}$ represents the river salt transport.

Note that either term on the right-hand side of Eq. (20) multiplied by $s_{\rm in}$ is equal to one of the long-term average mixing approximations. In Puget Sound, $s_{\rm in}$ is approximately constant over time, with small variations of ~ 2 g kg⁻¹. Therefore, using the approximation $M \approx (Q_{\rm in} \Delta s) s_{\rm in}$, the mixing in Puget Sound is

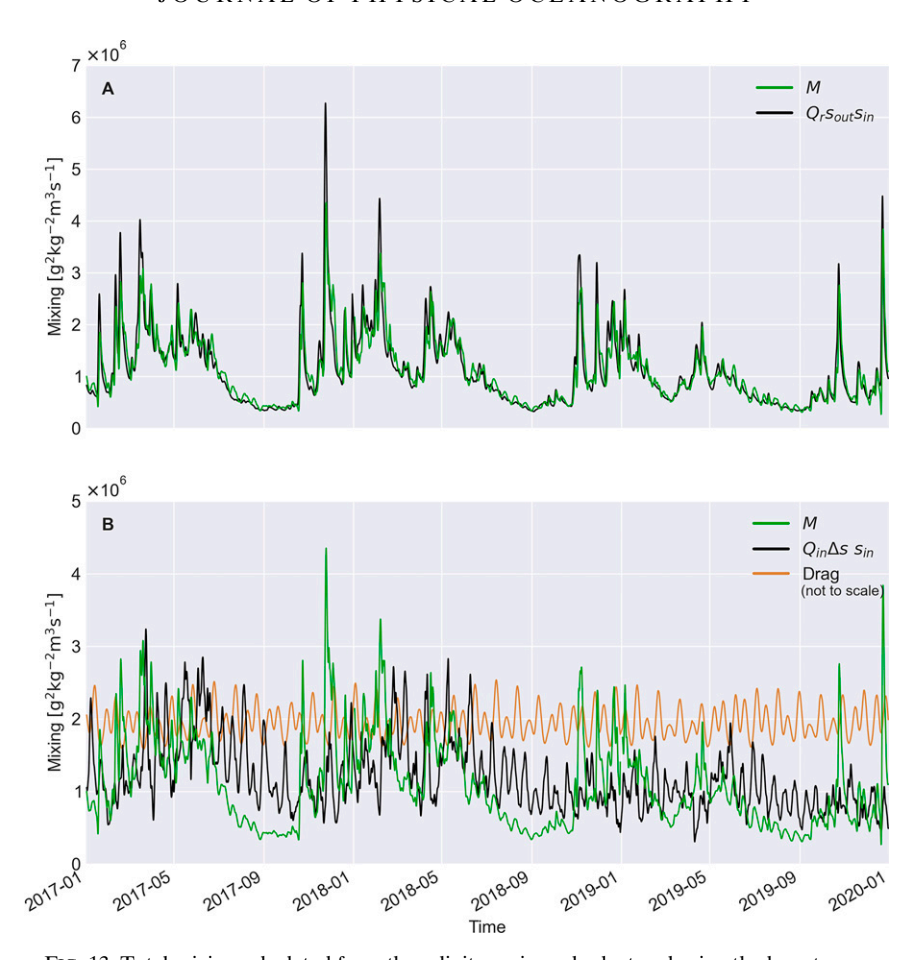


FIG. 13. Total mixing calculated from the salinity variance budget and using the long-term average approximations (a) $M = Q_{r}s_{out}s_{in}$ and (b) $M = Q_{in}\Delta ss_{in}$ in Puget Sound for 2017–19. The brown curve in (b) represents the spring–neap cycle (tidally averaged energy dissipation due to bottom drag, not to scale).

proportional to the exchange flow salt transport. We noted in the introduction that the approximation $M \approx Q_{\rm in} \Delta s s_{\rm in}$ provides an inexplicit link between mixing and the estuarine exchange flow. However, in systems similar to Puget Sound it may be more useful to instead consider that the direct link is between mixing and the exchange flow salt transport.

The $Q_r s_{out} s_{in}$ approximation can also be used to calculate the mixing completeness $M/(Q_r s_{in}^2)$, which is the ratio of total mixing to theoretical maximum mixing (MacCready et al. 2018). Using the 3-yr average values of mixing, river flow, s_{in} , and s_{out} , the mixing completeness in Puget Sound is 94.1%. This is high compared to values of mixing completeness found in studies of other estuaries. For example, (MacCready et al. 2018) found 68% mixing completeness in their idealized V-shaped estuary model, and Lange et al. (2020) found 84% mixing completeness in a modeling study of the weakly tidal Warnow estuary.

5. Summary

Using salinity variance budgets, we have gained insights into how mixing occurs in the Salish Sea. Most mixing occurs in the Strait of Georgia where the volume-normalized mixing

is close to the average for whole Salish Sea, due to its large size. The volume-normalized mixing is lower in the Strait of Juan de Fuca and higher in Puget Sound, although these two regions make similarly sized contributions to the total mixing. The strongest mixing by far occurs in Whidbey Basin, likely due to its shallow depth and large river flow. The timing of mixing in all regions of the Salish Sea is highly correlated with the river flow, whose annual cycle depends on whether the watershed is snow-dominated, rain-dominated or mixed. Because \bar{s} is close to the oceanic salinity in the Salish Sea, the rivers have very high variance and dominate the input of salinity variance to the estuary even though their volume transport is low. Unlike other estuaries studied using the salinity variance framework, no pronounced spring-neap cycle is seen in the mixing time series for the Salish Sea. Using the outflowing mixedness transport we determine that mixed water is also removed from the estuary when river flow is high, but the coupling is not as tight as it is between the river flow and mixing. Even without any additional time-averaging, the longterm average mixing approximation $M = Q_r s_{out} s_{in}$ can accurately predict the mixing in the Salish Sea and Puget Sound. Because the mixing is tightly coupled with the river flow and the $s_{\rm in}$ and $s_{\rm out}$ do not vary widely over time, additional averaging does not significantly improve the performance of this long-term average approximation. Over a long time average, the alternative approximation $M=Q_{\rm in}\Delta s s_{\rm in}$ may also be used to estimate the mixing in Puget Sound. Because $s_{\rm in}$ is nearly constant for Puget Sound, the average mixing in Puget Sound is directly proportional to the average exchange flow salt transport $Q_{\rm in}\Delta s$. The residual of the salinity variance budget gives an estimate of the numerical mixing, which accounts for approximately one-third of the total mixing in our model.

Acknowledgments. This project was supported by NSF Award 1736242: Using Salinity Variance to Link Estuarine Mixing and Exchange Flow. We thank W. Rockwell Geyer for the mixedness concept.

Data availability statement. All code used in this analysis is archived at https://doi.org/10.5281/zenodo.6568187, including code for calculating salinity variance budgets, salinity variance reservoirs, and forcing factor time series. Output data files and plotting code are also included. The LiveOcean model code is archived at https://doi.org/10.5281/zenodo.4282775 (MacCready et al. 2021).

APPENDIX

Derivation of Salinity Variance Budget from Diagnostics

To create a salinity variance budget from ROMS averages and diagnostics files, we start with a salt budget:

where salt_xavd, salt_yavd, and salt_vavd are diagnostics that give the rates of change due to advection in the x, y, and z directions, respectively, and salt_hdiff and salt_vdiff are diagnostics that give the rates of change due to horizontal and vertical diffusion, respectively. Salt_rate is the total rate of change in the salt content of the model cell, defined in ROMS as

$$salt_rate \equiv \frac{\left\langle \frac{\partial}{\partial t} (\delta s) \right\rangle}{\langle \delta \rangle}, \tag{A2}$$

where δ is the thickness of the cell and angle brackets represent averaging over the hour. Since the model has 30 terrain following vertical layers, the cell thickness changes over time as the sea surface height changes. In the interest of physical interpretability, we will apply a thickness correction to the budget in Eq. (A1) to account for this effect. Dropping the angle brackets and following MacCready and Giddings (2016), Eq. (A2) can be expanded as

$$salt_rate = \frac{\delta \frac{\partial s}{\partial t} + s \frac{\partial \delta}{\partial t}}{\delta},$$
 (A3)

$$\frac{\partial s}{\partial t} = \text{salt_rate} - \frac{s}{\delta} \frac{\partial \delta}{\partial t}.$$
 (A4)

The values of s and δ are taken from the averages files, while the derivative $\partial \delta/\partial t$ is calculated from the history files at the start and end of the hour. The final term in Eq. (A4) is the thickness correction that we apply to both sides of Eq. (A1):

$$salt_rate - \frac{s}{\delta} \frac{\partial \delta}{\partial t}$$

$$= salt_xavd + salt_yavd + \left(salt_vavd - \frac{s}{\delta} \frac{\partial \delta}{\partial t} \right)$$

$$+ salt_hdiff + salt_vdiff. \tag{A5}$$

Now the left-hand side is equal to $\partial \delta/\partial t$. We have grouped the thickness correction with the vertical advection on the right-hand side since the moving cell boundaries artificially change the advection though the top and bottom of the cell. Similarly to the development in section 2a, to create a salinity variance budget we multiply both sides of the equation by 2s':

$$2s' \left[\text{salt_rate} - \frac{s}{\delta} \frac{\partial \delta}{\partial t} \right]$$

$$= 2s' \left[\text{salt_xavd} + \text{salt_yavd} + \left(\text{salt_vavd} - \frac{s}{\delta} \frac{\partial \delta}{\partial t} \right) \right]$$

$$+ 2s' \left[\text{salt_hdiff} + \text{salt_vdiff} \right]. \tag{A6}$$

This equation balances exactly in every model cell. If we take the volume integral over the same volume V used to calculate \bar{s} ,

$$\int_{V} 2s' \left[\text{salt_rate} - \frac{s}{\delta} \frac{\partial \delta}{\partial t} \right] dV$$

$$= \int_{V} 2s' \left[\text{salt_xavd} + \text{salt_yavd} + \left(\text{salt_vavd} - \frac{s}{\delta} \frac{\partial \delta}{\partial t} \right) \right] dV$$

$$+ \int_{V} 2s' \left[\text{salt_hdiff} + \text{salt_vdiff} \right] dV. \tag{A7}$$

This is the salinity variance budget constructed from averages and diagnostics. Note that the integrand on the left-hand side of Eq. (A7) is $2s' \partial s/\partial t$. Similarly to section 2a, we can expand $s = \overline{s} + s'$:

$$\int_{V} 2s' \frac{\partial s}{\partial t} dV = \int_{V} 2s' \frac{\partial \overline{s}}{\partial t} dV + \int_{V} 2s' \frac{\partial s'}{\partial t} dV.$$
 (A8)

The first term on the right-hand side of Eq. (A8) can be eliminated since \bar{s} has no spatial gradients and the volume integral of s' is zero by definition. Therefore,

$$\int_{V} 2s' \, \frac{\partial s}{\partial t} \, dV = \int_{V} 2s' \, \frac{\partial s'}{\partial t} \, dV. \tag{A9}$$

Using the inverse product rule, we can reformulate the right-hand side of Eq. (A9):

$$\int_{V} 2s' \, \frac{\partial s}{\partial t} \, dV = \int_{V} \frac{\partial}{\partial t} (s'^2) \, dV. \tag{A10}$$

This means that

$$\int_{V} 2s' \left[\text{salt_rate} - \frac{s}{\delta} \frac{\partial \delta}{\partial t} \right] dV = \int_{V} \frac{\partial}{\partial t} (s'^2) dV.$$
 (A11)

The diagnostic advection fields in each direction give the change in the salt content of a cell due to the difference in salt fluxes through opposite cell walls. Therefore, the integrand of first term on the right-hand side of Eq. (A7) is a divergence:

$$2s' \left[\text{salt_xavd} + \text{salt_yavd} + \left(\text{salt_vavd} - \frac{s}{\delta} \frac{\partial \delta}{\partial t} \right) \right]$$
$$= -2s' \nabla \cdot (\mathbf{u}s), \tag{A12}$$

and if we assume incompressibility,

$$2s' \left[\text{salt_xavd} + \text{salt_yavd} + \left(\text{salt_vavd} - \frac{s}{\delta} \frac{\partial \delta}{\partial t} \right) \right]$$
$$= -2s' \mathbf{u} \cdot \nabla s. \tag{A13}$$

Again using the inverse product rule, we obtain

$$2s' \left[\text{salt_xavd} + \text{salt_yavd} + \left(\text{salt_vavd} - \frac{s}{\delta} \frac{\partial \delta}{\partial t} \right) \right]$$
$$= -\mathbf{u} \cdot \nabla (s'^2), \tag{A14}$$

and taking the volume integral produces

$$\int_{V} 2s' \left[\text{salt_xavd} + \text{salt_yavd} + \left(\text{salt_vavd} - \frac{s}{\delta} \frac{\partial \delta}{\partial t} \right) \right] dV$$

$$= -\int_{V} \mathbf{u} \cdot \nabla (s')^{2} dV. \tag{A15}$$

Substituting Eq. (A11) and Eq. (A15) into the diagnostics budget Eq. (A7) we find

$$\int_{V} \left[\frac{\partial}{\partial t} (s'^{2}) + \mathbf{u} \cdot \nabla (s'^{2}) \right] dV$$

$$= \int_{V} 2s' [\text{salt_hdiff} + \text{salt_vdiff}] dV. \quad (A16)$$

Using the same reasoning as presented in section 2a, we can move the derivative on the right-hand side outside the integral due to the Reynolds transport theorem:

$$\frac{d}{dt} \int_{V} (s'^{2}) dV = -\int_{A} s'^{2} \mathbf{u} \cdot \hat{\mathbf{n}} dA$$

$$+ \int_{V} 2s' [\text{salt_hdiff} + \text{salt_vdiff}] dV. \quad (A17)$$

Now we can see that Eq. (A7) is an exact salinity variance budget constructed from the diagnostics with three terms:

Storage = Advection + Diffusion,
$$(A18)$$

where

Storage:
$$\int_{V} 2s' \left[\text{salt_rate} - \frac{s}{\delta} \frac{\partial \delta}{\partial t} \right] dV, \tag{A19}$$

Advection:
$$\int_{V} 2s' \left[\text{salt_xavd} + \text{salt_yavd} \right]$$

$$+ \left(\text{salt_vavd} - \frac{s}{\delta} \frac{\partial \delta}{\partial t} \right) dV, \tag{A20}$$

Mixing:
$$\int_{V} 2s'[\text{salt_hdiff} + \text{salt_vdiff}]dV$$
. (A21)

REFERENCES

- Burchard, H., and H. Rennau, 2008: Comparative quantification of physically and numerically induced mixing in ocean models. *Ocean Modell.*, 20, 293–311, https://doi.org/10.1016/j.ocemod. 2007.10.003.
- —, F. Janssen, K. Bolding, L. Umlauf, and H. Rennau, 2009: Model simulations of dense bottom currents in the western Baltic Sea. *Cont. Shelf Res.*, 29, 205–220, https://doi.org/10. 1016/j.csr.2007.09.010.
- —, and Coauthors, 2018: The Knudsen theorem and the total exchange flow analysis framework applied to the Baltic Sea. *Prog. Oceanogr.*, 165, 268–286, https://doi.org/10.1016/j.pocean. 2018.04.004.
- —, X. Lange, K. Klingbeil, and P. MacCready, 2019: Mixing estimates for estuaries. J. Phys. Oceanogr., 49, 631–648, https:// doi.org/10.1175/JPO-D-18-0147.1.
- Casola, J., J. Kay, A. Snover, R. Norheim, and L. Whitely Binder, 2005: Climate impacts on Washington's hydropower, water supply, forests, fish, and agriculture. Tech. Rep., 43 pp., https:// doi.org/10.7915/CIG9C53GK.
- Cokelet, E. D., and R. J. Stewart, 1985: The exchange of water in fjords: The efflux/reflux theory of advective reaches separated by mixing zones. *J. Geophys. Res.*, 90, 7287–7306, https://doi. org/10.1029/JC090iC04p07287.
- Ebbesmeyer, C. C., J. Q. Word, and C. A. Barnes, 1988: Puget Sound: A fjord system homogenized with water recycled over sills by tidal mixing. *Hydrodynamics of Estuaries: Volume II Estuarine Case Studies*, B. Kjerfve, Ed., CRC Press, 17–29, https://doi.org/10.1201/9781351073264.
- Geyer, W. R., and G. A. Cannon, 1982: Sill processes related to deep water renewal in a fjord. J. Geophys. Res., 87, 7985– 7996, https://doi.org/10.1029/JC087iC10p07985.
- Giddings, S. N., and P. MacCready, 2017: Reverse estuarine circulation due to local and remote wind forcing, enhanced by the presence of along-coast estuaries. *J. Geophys. Res. Oceans*, 122, 10184–10205, https://doi.org/10.1002/2016JC012479.
- Godin, G., 1972: The Analysis of Tides. University of Toronto Press, 264 pp.
- Knudsen, M., 1900: Ein hydrographischer Lehrsatz. Ann. Hydrogr. Marit. Meteor., 28, 316–320
- Lange, X., K. Klingbeil, and H. Burchard, 2020: Inversions of estuarine circulation are frequent in a weakly tidal estuary with variable wind forcing and seaward salinity fluctuations. *J. Geophys. Res. Oceans*, 125, e2019JC015789, https://doi.org/10.1029/2019JC015789.
- Lee, S.-Y., and A. F. Hamlet, 2011: Skagit River basin climate science report. Tech. Rep., 226 pp., https://www.skagitcounty.net/EnvisionSkagit/Documents/ClimateChange/Complete.pdf.

- Li, X., W. R. Geyer, J. Zhu, and H. Wu, 2018: The transformation of salinity variance: A new approach to quantifying the influence of straining and mixing on estuarine stratification. *J. Phys. Oceanogr.*, 48, 607–623, https://doi.org/10.1175/JPO-D-17-0189.1.
- Lorenz, M., K. Klingbeil, P. MacCready, and H. Burchard, 2019: Numerical issues of the total exchange flow (TEF) analysis framework for quantifying estuarine circulation. *Ocean Sci.*, **15**, 601–614, https://doi.org/10.5194/os-15-601-2019.
- MacCready, P., 2011: Calculating estuarine exchange flow using isohaline coordinates. J. Phys. Oceanogr., 41, 1116–1124, https://doi.org/10.1175/2011JPO4517.1.
- —, and S. N. Giddings, 2016: The mechanical energy budget of a regional ocean model. *J. Phys. Oceanogr.*, 46, 2719–2733, https://doi.org/10.1175/JPO-D-16-0086.1.
- ——, W. R. Geyer, and H. Burchard, 2018: Estuarine exchange flow is related to mixing through the salinity variance budget. *J. Phys. Oceanogr.*, 48, 1375–1384, https://doi.org/10.1175/ JPO-D-17-0266.1.
- —, and Coauthors, 2021: Estuarine circulation, mixing, and residence times in the Salish Sea. *J. Geophys. Res. Oceans*, 126, e2020JC016738, https://doi.org/10.1029/2020JC016738.
- Peters, H., and R. Bokhorst, 2001: Microstructure observations of turbulent mixing in a partially mixed estuary. Part II: Salt flux and stress. J. Phys. Oceanogr., 31, 1105–1119, https://doi. org/10.1175/1520-0485(2001)031<1105:MOOTMI>2.0.CO;2.
- Ralston, D. K., G. W. Cowles, and W. R. Geyer, 2017: Turbulent and numerical mixing in a salt wedge estuary: Dependence on grid resolution, bottom roughness, and turbulence closure. *J. Geophys. Res. Oceans*, 122, 692–712, https://doi.org/10. 1002/2016JC011738.
- SeaDoc Society, 2021: About the Salish Sea. https://www.seadocsociety.org/about-the-salish-sea.

- Simpson, J. H., J. Brown, J. Matthews, and G. Allen, 1990: Tidal straining, density currents, and stirring in the control of estuarine stratification. *Estuaries*, 13, 125–132, https://doi.org/10. 2307/1351581.
- Thomson, R. E., S. F. Mihály, and E. A. Kulikov, 2007: Estuarine versus transient flow regimes in Juan de Fuca Strait. J. Geophys. Res., 112, C09022, https://doi.org/10.1029/2006JC003925.
- Walters, R. A., and C. Heston, 1982: Removing tidal-period variations from time-series data using low-pass digital filters. *J. Phys. Oceanogr.*, 12, 112–115, https://doi.org/10.1175/1520-0485(1982)012<0112:RTPVFT>2.0.CO;2.
- Wang, T., and W. R. Geyer, 2018: The balance of salinity variance in a partially stratified estuary: Implications for exchange flow, mixing, and stratification. *J. Phys. Oceanogr.*, 48, 2887– 2899, https://doi.org/10.1175/JPO-D-18-0032.1.
- —, and P. MacCready, 2017: Total exchange flow, entrainment, and diffusive salt flux in estuaries. *J. Phys. Oceanogr.*, 47, 1205–1220, https://doi.org/10.1175/JPO-D-16-0258.1.
- —, Z. Wei, W. Jiang, T. Xu, J. L. Chen, and C. Bian, 2021: Quantification of numerical mixing in coastal ocean models through an offline method. *Ocean Eng.*, 222, 108588, https://doi.org/10.1016/j.oceaneng.2021.108588.
- Warner, J. C., W. R. Geyer, D. K. Ralston, and T. Kalra, 2020: Using tracer variance decay to quantify variability of salinity mixing in the Hudson River estuary. *J. Geophys. Res. Oceans*, 125, e2020JC016096, https://doi.org/10.1029/2020JC016096.
- Yu, Z., Y. Fan, E. J. Metzger, and O. M. Smedstad, 2018: The wind work input into the global ocean revealed by a 17-year global hybrid coordinate ocean model reanalysis. *Ocean Modell.*, 130, 29–39, https://doi.org/10.1016/j.ocemod.2018.07.